Comparative study of high-order positivity-preserving WENO schemes

By D.V. Kotov, H.C. Yee AND B. Sjögreen

1. Motivation and objectives

In gas dynamics and magnetohydrodynamics flows, physically, the density ρ and the pressure p should both be positive. In a standard conservative numerical scheme, however, the computed internal energy is obtained by subtracting the kinetic energy from the total energy, resulting in a computed p that may be negative. Examples are problems in which the dominant energy is kinetic. Negative ρ may often emerge in computing blast waves. In such situations the computed eigenvalues of the Jacobian will become imaginary. Consequently, the initial value problem for the linearized system will be ill posed. This explains why failure of preserving positivity of density or pressure may cause blow-ups of the numerical algorithm. The adhoc methods in numerical strategy which modify the computed negative density and/or the computed negative pressure to be positive are neither a conservative cure nor a stable solution. Conservative positivity-preserving schemes are more appropriate for such flow problems.

The ideas of Zhang & Shu (2012) and Hu *et al.* (2012) precisely address the aforementioned issue. Zhang & Shu constructed a new conservative positivity-preserving procedure to preserve positive density and pressure for high-order WENO schemes by the Lax-Friedrichs flux (WENO/LLF). In general, WENO/LLF is too dissipative for flows such as turbulence with strong shocks computed in direct numerical simulations (DNS) and large eddy simulations (LES). The new conservative positivity-preserving procedure proposed in Hu *et al.* (2012) can be used with any high-order shock-capturing scheme, including high-order WENO schemes using the Roe's flux (WENO/Roe).

The goal of this study is to compare the results obtained by non-positivity-preserving methods with the recently developed positivity-preserving schemes for representative test cases. In particular the more difficult 3D Noh and Sedov problems are considered. These test cases are chosen because of the negative pressure/density most often exhibited by standard high-order shock-capturing schemes. The simulation of a hypersonic nonequilibrium viscous shock tube that is related to the NASA Electric Arc Shock Tube (EAST) is also included. EAST is a high-temperature and high Mach number viscous nonequilibrium flow consisting of 13 species. In addition, as most common shock-capturing schemes have been developed for problems without source terms, when applied to problems with nonlinear and/or stiff source terms these methods can result in spurious solutions, even when solving a conservative system of equations with a conservative scheme. This kind of behavior can be observed even for a scalar case (LeVeque & Yee 1990) as well as for the case consisting of two species and one reaction (Wang *et al.* 2012). For further information concerning this issue see (LeVeque & Yee 1990; Griffiths *et al.* 1992; Lafon & Yee 1996; Yee *et al.* 2012). This EAST example indicated that standard high-order shock-capturing methods exhibit instability of density/pressure in addition to grid-dependent discontinuity locations with insufficient grid points. The evaluation

of these test cases is based on the stability of the numerical schemes together with the accuracy of the obtained solutions.

2. Positivity-preserving algorithms

Here we briefly describe the positivity-preserving method of Hu *et al.* (2012). Readers are referred to Zhang & Shu (2012) for their positivity-preserving WENO schemes that are valid only for the Lax-Friedrichs flux formulation. Consider the Euler equations:

$$\mathbf{w}_t + \mathbf{f}(\mathbf{w})_x = 0, \tag{2.1}$$

$$\mathbf{w} = \begin{pmatrix} \rho \\ m \\ E \end{pmatrix}, \quad \mathbf{f}(\mathbf{w}) = \begin{pmatrix} m \\ \rho u^2 + p \\ (E+p)u \end{pmatrix} \tag{2.2}$$

with

$$m = \rho u, \quad E = \frac{1}{2}\rho u^2 + \rho e, \quad p = (\gamma - 1)\rho e,$$

where ρ is the density, u is the velocity, m is the momentum, E is the total energy, p is the pressure, e is the internal energy, and $\gamma > 1$ is a constant. The speed of sound is given by $c = \sqrt{\gamma p/\rho}$ and the three eigenvalues of the Jacobian $\mathbf{f}'(\mathbf{w})$ are $u - c$, u and $u + c$.

A general explicit k^{th}-order conservative scheme with Euler-forward time integration for Eq. (2.1) can be written as

$$\mathbf{w}_i^{n+1} = \mathbf{w}_i^n - \lambda \left(\widehat{\mathbf{f}}_{i+\frac{1}{2}} - \widehat{\mathbf{f}}_{i-\frac{1}{2}} \right), \tag{2.3}$$

where the superscripts n and $n+1$ represent the old and new time-steps, respectively, and $\lambda = \Delta t/\Delta x$, where Δt is the time-step size and Δx is the grid-step size.

Eq. (2.3) can be rewritten as follows:

$$2\mathbf{w}_i^{n+1} = \left(\mathbf{w}_i^n + 2\lambda \widehat{\mathbf{f}}_{i-\frac{1}{2}} \right) + \left(\mathbf{w}_i^n - 2\lambda \widehat{\mathbf{f}}_{i+\frac{1}{2}} \right) = \mathbf{w}_i^+ + \mathbf{w}_i^-. \tag{2.4}$$

The positivity-preserving procedure of Hu et al. involves the first-order Lax-Friedrichs scheme with numerical flux:

$$\widehat{\mathbf{f}}_{i+\frac{1}{2}}^{LF} = \frac{1}{2}\left[\mathbf{f}_i + \mathbf{f}_{i+1} + (|u| + c)_{max} \left(\mathbf{w}_i^n - \mathbf{w}_{i+1}^n \right) \right]. \tag{2.5}$$

Let $\mathbf{w}_i^{LF,\pm} = \mathbf{w}_i^n \mp 2\lambda \widehat{\mathbf{f}}_{i+\frac{1}{2}}^{LF}$. The positive density is first enforced by the following **cut-off flux limiter for positive density:**

1. For all i initialize $\theta_{i+1/2}^+ = 1, \theta_{i+1/2}^- = 1$.

2. If $\rho\left(\mathbf{w}_i^+\right) < \epsilon_\rho$, solve $\theta_{i+1/2}^+$ from $(1 - \theta_{i+1/2}^+)\rho(\mathbf{w}_i^{LF,+}) + \theta_{i+1/2}^+ \rho(\mathbf{w}_i^+) = \epsilon_\rho$.

3. If $\rho\left(\mathbf{w}_i^-\right) < \epsilon_\rho$, solve $\theta_{i+1/2}^-$ from $(1 - \theta_{i+1/2}^-)\rho(\mathbf{w}_i^{LF,-}) + \theta_{i+1/2}^- \rho(\mathbf{w}_i^-) = \epsilon_\rho$.

4. Set $\theta_{\rho,i+1/2} = \min(\theta_{i+1/2}^+, \theta_{i+1/2}^-)$, $\widehat{\mathbf{f}}_{i+\frac{1}{2}}^* = (1 - \theta_{\rho,i+1/2}^-)\widehat{\mathbf{f}}_{i+\frac{1}{2}}^{LF} + \theta_{\rho,i+1/2}^- \widehat{\mathbf{f}}_{i+\frac{1}{2}}$.

Here, $\epsilon_\rho = \min\{10^{-13}, \rho_{min}^0\}$, where ρ_{min}^0 is the minimum density in the initial condition, $\widehat{\mathbf{f}}_{i+\frac{1}{2}}^*$ is the limited flux, and $0 \le \theta_{i+1/2}^\pm \le 1$ are the limiting factors corresponding to the two neighboring cells, which share the same flux $\widehat{\mathbf{f}}_{i+\frac{1}{2}}$. After applying this flux limiter, Eq. (2.4) becomes

$$2\mathbf{w}_i^{n+1} = \left(\mathbf{w}_i^n + 2\lambda \widehat{\mathbf{f}}_{i-\frac{1}{2}}^* \right) + \left(\mathbf{w}_i^n - 2\lambda \widehat{\mathbf{f}}_{i+\frac{1}{2}}^* \right) = \mathbf{w}_i^{*,+} + \mathbf{w}_i^{*,-}. \tag{2.6}$$

The positive pressure is further enforced by the following **cut-off flux limiter for positive pressure:**

1. For all i initialize $\theta^+_{i+1/2} = 1, \theta^-_{i+1/2} = 1$.

2. If $p\left(\mathbf{w}^+_i\right) < \epsilon_p$, solve $\theta^+_{i+1/2}$ from $(1-\theta^+_{i+1/2})p(\mathbf{w}^{LF,+}_i) + \theta^+_{i+1/2}p(\mathbf{w}^{*,+}_i) = \epsilon_p$.

3. If $p\left(\mathbf{w}^-_i\right) < \epsilon_p$, solve $\theta^-_{i+1/2}$ from $(1-\theta^-_{i+1/2})p(\mathbf{w}^{LF,-}_i) + \theta^-_{i+1/2}p(\mathbf{w}^{*,-}_i) = \epsilon_p$.

4. Set $\theta_{p,i+1/2} = \min(\theta^+_{i+1/2}, \theta^-_{i+1/2})$, $\widehat{\mathbf{f}}^{**}_{i+\frac{1}{2}} = (1-\theta^-_{p,i+1/2})\widehat{\mathbf{f}}^{LF}_{i+\frac{1}{2}} + \theta^-_{p,i+1/2}\widehat{\mathbf{f}}^{*}_{i+\frac{1}{2}}$.

Again, $\epsilon_p = \min\{10^{-13}, p^0_{min}\}$, where p^0_{min} is the minimum pressure in the initial condition, and $\widehat{\mathbf{f}}^{**}_{i+\frac{1}{2}}$ is the further limited flux. With these limited fluxes, the original scheme (2.3) is modified as

$$\mathbf{w}^{n+1}_i = \mathbf{w}^n_i - \lambda\left(\widehat{\mathbf{f}}^{**}_{i+\frac{1}{2}} - \widehat{\mathbf{f}}^{**}_{i-\frac{1}{2}}\right). \tag{2.7}$$

The above new procedure can be applied at each sub-stage of a TVD Runge-Kutta (Shu & Osher 1988) method, which is a convex combination of Euler-forward time-steps. Note that any high-order numerical flux can be used in this formulation.

3. Numerical results

The numerical experiments include 1D and 3D Noh problems, 3D Sedov blast, a Mach 2000 jet test case, and the 1D EAST hypersonic viscous nonequilibrium shock tube. The comparative study includes the following numerical schemes:

- UPWIND - first-order upwind scheme using Roe average state;
- TVD - second-order TVD (Yee 1989; Yee *et al.* 1990);
- Standard fifth- and seventh-order WENO (WENO5 and WENO7) with local Lax-Friedrichs flux (WENO5-LLF and WENO7-LLF) and Roe flux (WENO5-Roe), see Jiang & Shu (1996);
- WENO5fi+split and WENO7fi+split - high-order nonlinear filter counterparts of WENO5 and WENO7 using the wavelet flow sensor in conjunction with the Ducros et al. splitting of the inviscid flux derivatives (see Yee & Sjögreen (2007, 2010));
- Zhang & Shu positivity-preserving WENO5 and WENO7 local Lax-Friedrichs flux (WENO5P, WENO7P) and of fifth order with global Lax-Friedrichs flux (WENOGP);
- Hu et al. positivity-preserving WENO5 with local Lax-Friedrichs flux (WENO5PH) and Roe's flux (WENO5PH-Roe). Similarly for WENO5Pfi+split.

Note that for the TVD scheme, Roe's average state is employed.

3.1. *The Noh problem*

The first test case is the well-known 1D and 3D spherical Noh implosion problem (Noh 1987). The initial conditions are $\rho = 1$, $p = 0$ and $u =$ unit vector directed toward the origin with $\gamma = 5/3$. In this problem an infinite-strength shock expands outward from the origin at a constant velocity of 1/3. The goal is to test the ability of the scheme to preserve spherical symmetry and produce the correct entropy jump for adiabatic shock compression.

The results obtained using different schemes for the 1D case are shown in Figure 1. The grid size is $h = 0.002$. The second-order TVD scheme appears to be not stable for the chosen limiter and entropy fix. Increasing the order of the WENO scheme from fifth to seventh-order gives slightly better results. In addition, the regular WENO-LLF schemes are slightly more accurate than their positive counterparts. WENO5-Roe performs with

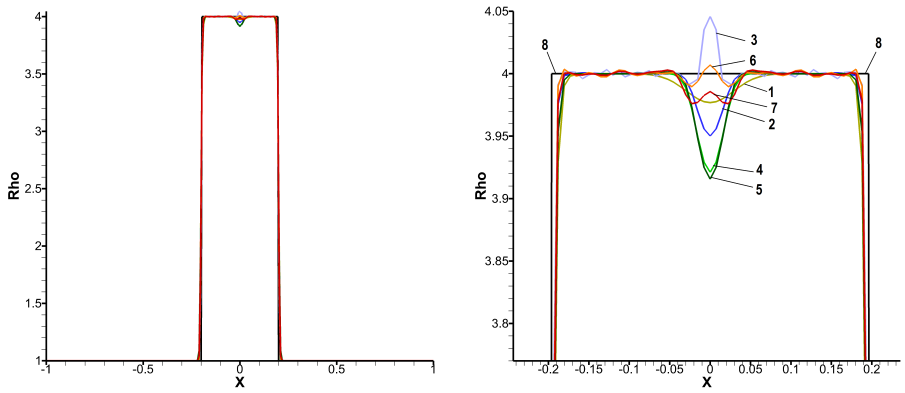

FIGURE 1. Density plot for the Noh-1D problem obtained by UPWIND (line 1), WENO5-LLF (line 2), WENO5-Roe (line 3), WENO5GP (line 4), WENO5P (line 5), WENO7-LLF (line 6), WENO7P (line 7) on a grid $N = 267$. Reference solution: line 8. The right figure is zoomed in the vicinity of $x = 0$.

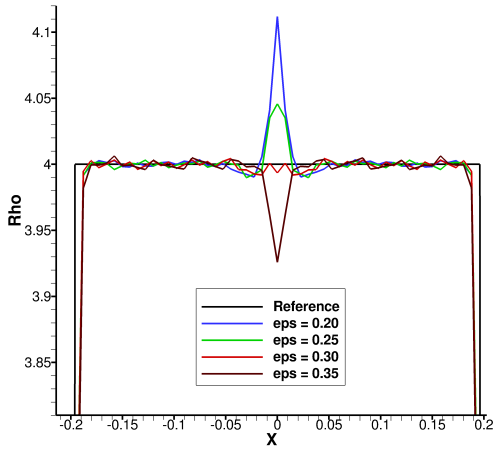

FIGURE 2. Density plot for the Noh-1D problem obtained by WENO5-Roe on a grid $N = 267$ with different values of the entropy fix parameter: $\epsilon = 0.20$ (line 1), $\epsilon = 0.25$ (line 2), $\epsilon = 0.30$ (line 3), $\epsilon = 0.35$ (line 4). Reference solution: line 5.

the same accuracy as WENO5-LLF using a large entropy fix. Its accuracy can be improved by using the appropriate entropy fix parameter ϵ. Figure 2 shows the results by WENO5-Roe with different values of ϵ. The value $\epsilon = 0.3$ produces an error close to zero in the vicinity of $x = 0$ instead of an error of 0.5% obtained by the scheme with a value of $\epsilon = 0.25$.

The 2D slices at $z = 0$ obtained for the 3D case by UPWIND, WENO5P, WENO7P, WENO5PH, WENO7PH and WENO5PH-Roe are shown in Figure 3. The grid size is $134 \times 134 \times 134$. Note that regular WENO5-LLF and WENO5-Roe are not stable for the Noh 3D problem due to computed negative pressure/density. The results by WENO5P and WENO7P also contain some points with small negative pressure values. This can be fixed by applying an adaptive time-step that uses the positivity-preservation condition. The results obtained using WENO5PH, WENO5PH-Roe and WENO7PH with

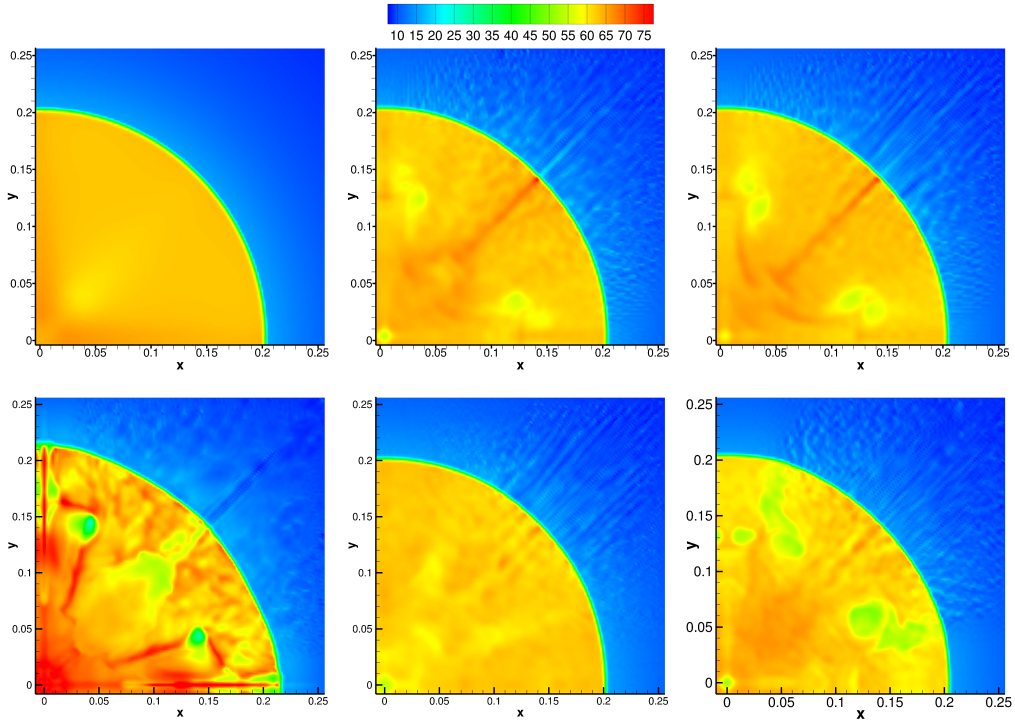

FIGURE 3. Density contours for the Noh-3D problem on a grid $134 \times 134 \times 134$, slice $z = 0$. Top row: UPWIND, WENO5P and WENO7P. Bottom row: WENO5PH-Roe, WENO5PH and WENO7PH.

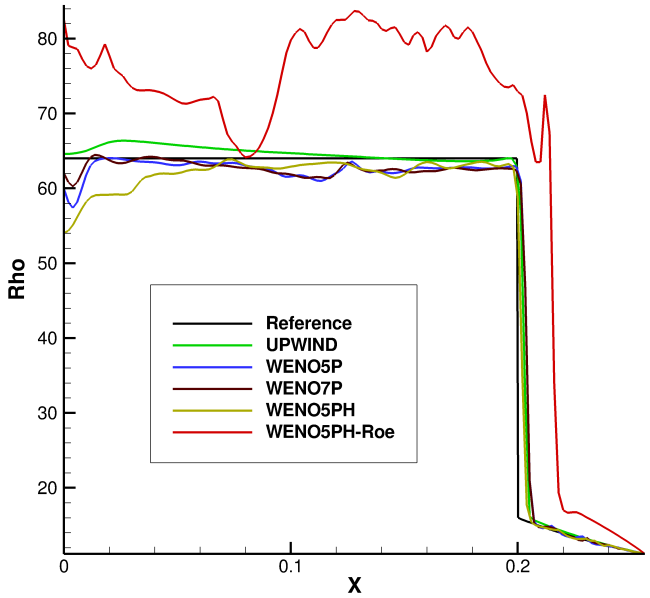

FIGURE 4. Comparison of the results for the Noh-3D problem obtained by UPWIND (line 1), WENO5P (line 2), WENO7P (line 3), WENO5PH (line 4) and WENO5PH-Roe (line 5) with the reference solution (line 6) for the slice $y = 0, z = 0$ on a grid $134 \times 134 \times 134$.

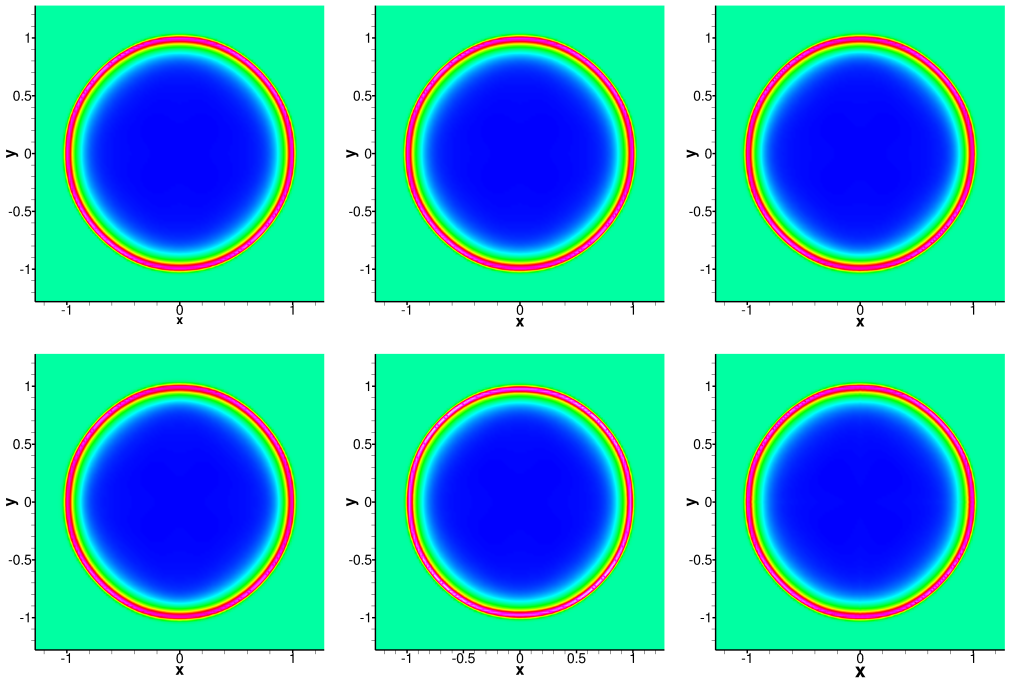

FIGURE 5. Density contours for the Sedov-3D problem on a grid $128 \times 128 \times 128$ (slice $z = 0$). Top row: WENO5-LLF, WENO5Pfi+split and WENO5PH. Bottom row: WENO5P, WENO7P and WENO5PH-Roe.

the same CFL exhibit positive density and pressure values. In the case of computation using WENO5PH-Roe, a high value $\epsilon = 0.5$ has been used to achieve an acceptable performance. Figure 4 shows a comparison of the results obtained using the same methods with the reference solution for the slice $y = 0, z = 0$. The increase of the scheme order from WENO5P to WENO7P does not improve the quality of the results for this problem. This is an expected behavior for cases where solutions are almost constant apart from discontinuities. Using Roe flux for WENO5PH leads to significant oscillations.

3.2. *The Sedov problem*

The second test case is the 3D spherical Sedov blast wave (Sedov 1959). The initial conditions are $\rho = 1$, $u = 0$ and $e = 0.1528415451 \exp(-R^2/R_0^2)/R_0^3$, where $R = \sqrt{x^2 + y^2 + z^2}$ and $R_0 = 2/h$. The grid size is $h = 0.02$ and $\gamma = 1.4$. The density and temperature contours are shown in Figs. 5 and 6. The deviation from spherical symmetry for positive schemes is bigger than for regular WENO, which is well observed on the temperature contours. However, the solution obtained using standard WENO schemes contains some points with small negative pressure values, whereas, WENOP and WENOPfi obtain all positive pressure and density values. Switching to Roe's flux causes even further deviation from symmetry (see results obtained using WENO5PH-Roe). Note that the density contours obtained by all of these methods look very similar.

3.3. *Mach 2000 jet*

The same Mach 2000 jet problem as that in Zhang & Shu (2010) is considered here with $\gamma = 5/3$. The computational domain is $[0, 1] \times [-0.25, 0.25]$. The initial flow condition

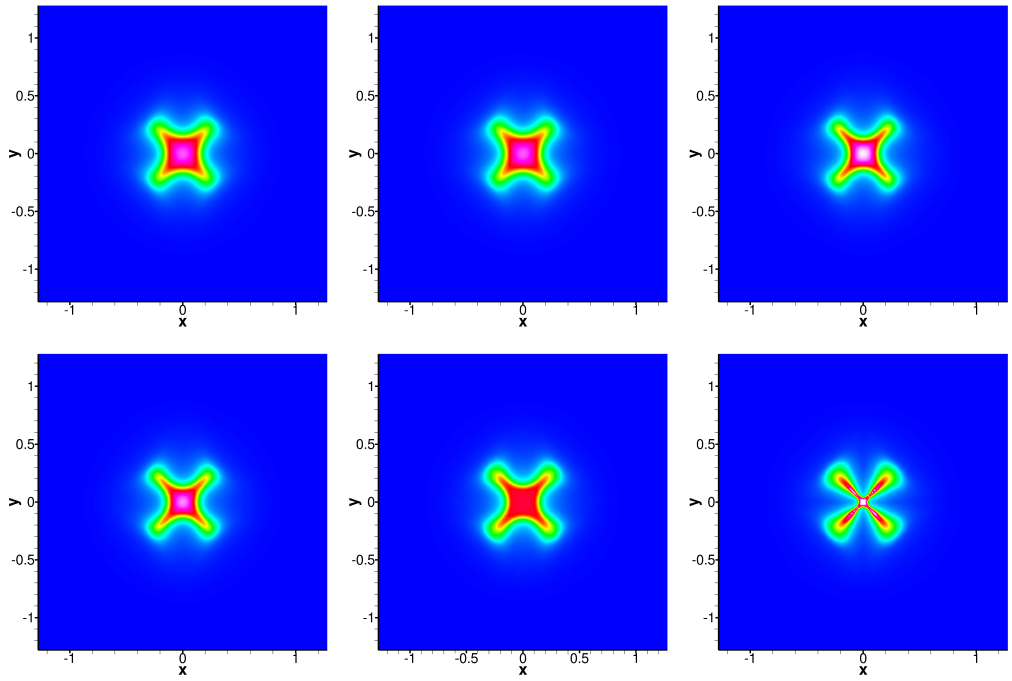

FIGURE 6. Temperature contours for the Sedov-3D problem on a grid $128 \times 128 \times 128$ (slice $z = 0$). Top row: WENO5-LLF, WENO5Pfi+split and WENO5PH. Bottom row: WENO5P, WENO7P and WENO5PH-Roe.

is the ambient gas with $(\rho, u, v, p) = (0.5, 0, 0, 0.4127)$. The boundary conditions for the right, top and bottom are outflow. For the left boundary, $(\rho, u, v, p) = (5, 800, 0, 0.4127)$ if $y \in [-0.05, 0.05]$ and $(\rho, u, v, p) = (0.5, 0, 0, 0.4127)$ otherwise. The terminal time is 0.001. The speed of the jet is 800, which is around Mach 2100 with respect to the sound speed in the jet gas.

For this problem a very small initial CFL value is required for high-order computation (about 0.01). For this reason, a variable time-step control is used in the computation. After each RK stage the solution is tested using the positivity condition. If the condition is not satisfied, the time-step is divided by a factor of 2 and the current RK step is repeated again. In this way the computation can be carried out with an average CFL value $4 - 8$ times larger than the fixed CFL.

The results by different schemes on the uniform grid 800×400 are shown in Figure 7. Note that regular WENO5-LLF, WENO5-Roe and their nonlinear filter counterparts WENO5fi+split exhibit negative pressure. In general, the quality of the results by positive WENO schemes increases as the order increases. The obtained results using WENO5PH-Roe are a little less dissipative than in the case using WENO5PH-LLF or WENO5P. The entropy fix parameter used in WENO5PH-Roe for this case was $\epsilon = 0.3$.

For the above 3D Noh and the Mach 2000 jet test cases, the nonlinear filter counterparts of WENO5P, WENO7P WENO5PH and WENO7PH are not stable due to the wide stencil of the wavelet flow sensor. Research is underway to develop a flow sensor with a more narrow stencil for such flows. Note that these filter counterparts are stable and

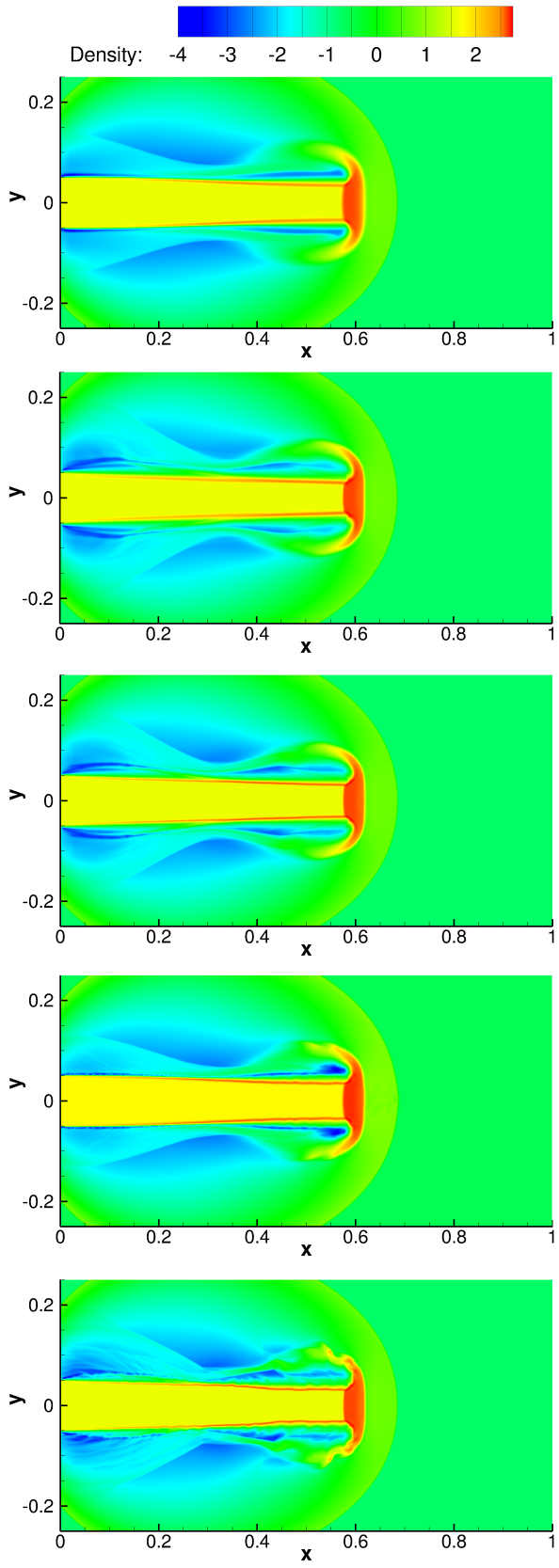

FIGURE 7. From top to bottom: density contours for the Mach 2000 jet problem obtained by TVD, WENO5GP, WENO5P, WENO5PH-Roe and WENO7P on a grid 800×400. Scales are logarithmic.

ρ	$1.10546\ kg/m^3$	ρ	$3.0964 \times 10^{-4} kg/m^3$
T	$6000\ K$	T	$300\ K$
p	$12.7116\ MPa$	p	$26.771\ Pa$
Y_{He}	0.9856	Y_{O_2}	0.21
Y_{N_2}	0.0144	Y_{N_2}	0.79

TABLE 1. High- (left) and low- (right) pressure region initial data

exhibit better accuracy than its non-filter counterparts for problems that do not have the aforementioned special extreme condition.

3.4. *13 species 1D EAST simulation*

The computational domain has a total length of $8.5m$. The left part of the domain with length $0.1m$ is a high-pressure region. The right part of the domain with length $8.4m$ is a low-pressure region. The gas mixture consists of 13 species:

$$e^-, He, N, O, N_2, NO, O_2, N_2^+, NO^+, N^+, O_2^+, O^+, He^+.$$

The initial conditions of the high- and low-pressure regions are listed in the Table 1. For the left-side boundary the Euler (slip) wall condition is applied, and for the right-side, the zero gradient condition is applied for all variables. As mentioned before, EAST is a high-temperature and high Mach number viscous non-equilibrium flow consisting of 13 species. In addition, as most common shock-capturing schemes have been developed for problems without source terms, when applied to problems with nonlinear and/or stiff source terms these methods can result in spurious solutions, even when solving a conservative system of equations with a conservative scheme. Here only selected schemes are used for this simulation.

Figure 8 shows the results from the computation using the Harten-Yee second-order TVD scheme (Yee 1989; Yee *et al.* 1990) for four grids with $\Delta x = 10^{-3}\ m$, $5\times10^{-4}\ m$, $5\times10^{-5}\ m$ and $2.5 \times 10^{-5}\ m$ at time $t_{end} = 0.325 \times 10^{-4}\ sec$. One can observe a significant shift in the shear (left discontinuity) and the shock (right discontinuity) locations as the grid is refined. The distance between the shear and the shock shrinks as the grid is refined. The difference between shock locations obtained on the grids with $\Delta x = 5 \times 10^{-5}\ m$ and $2.5\times10^{-5}\ m$ is less than 0.3%. Thus the solution using $\Delta x = 5\times10^{-5}\ m$ can be considered as the reference solution.

The left subfigure of Figure 9 shows a comparison among five methods obtained on a coarse grid ($\Delta x = 10^{-3}\ m$) with the reference solution. The scheme's labels are defined as follows:

- ACMTVDfi: Second-order central base scheme using ACM flow sensor. See Yee *et al.* (1999) for further information on filter schemes.
- WENO5-llf: Fifth-order WENO (WENO5) using the local Lax-Friedrichs flux.
- WENO5P-llf: Positive WENO5 of Zhang & Shu (2012) using the local Lax-Friedrichs flux.
- WENO5PH-llf: Positive WENO5 of Hu *et al.* (2012) using the local Lax-Friedrichs flux.

The right subfigure of Figure 9 shows a comparison of ACMTVDfi using a different weight κ parameter of the ACM flow sensor. The smaller the κ, the smaller the amount of TVD dissipation that is used. Among the considered schemes, Figure 9 indicates that the

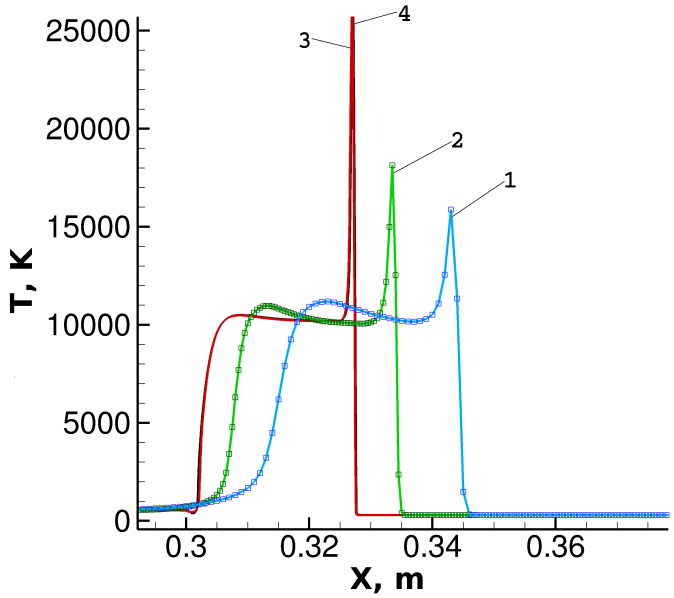

FIGURE 8. 13 species 1D EAST problem: Second-order Harten-Yee TVD simulation for three grids: $\Delta x = 10^{-3}$ m (line 1), 5×10^{-4} m (line 2), 5×10^{-5} m (line 3), 2.5×10^{-5} m (line 4), and $Tend = 0.325 \times 10^{-4} s$, with $CFL = 0.8$.

least dissipative scheme predicts the shear and shock locations best when compared with the reference solution. The results indicate that ACMTVDfi is slightly more accurate than WENO5-llf. This is due to the fact that ACMTVDfi reduces the amount of numerical dissipation away from high gradient regions. Using the subcell resolution method of Wang *et al.* (2012) for one reaction case by applying it to only one of the reactions in this multireaction flow does not improve the performance over standard schemes. Further research on the generalization of subcell resolution to multi-reactions needs to be explored.

4. Summary

The positivity-preserving schemes produce more stable behavior than regular WENO for the considered problems. The scheme by Hu *et al.* (2012) achieves slightly better positivity preservation than the scheme by Zhang & Shu (2012) using the same CFL number. These positivity-preserving schemes also are more diffusive than their standard WENO counterparts. Accuracy can be improved when using Roe's flux with the Hu et al. scheme instead of using Lax-Friedrichs, which is required by the Zhang-Shu scheme.

Acknowledgments

The support of the DOE/SciDAC SAP grant DE-AI02-06ER25796 is acknowledged. The work was performed with the first author as a postdoc fellow at the Center for Turbulence Research, Stanford University. The authors are grateful to X. Zhang and X. Y. Hu for providing their positive scheme routines. Financial support from the NASA Fundamental Aeronautics (Hypersonic) program for the second author is gratefully acknowledged. Work by the third author was performed under the auspices of the U.S.

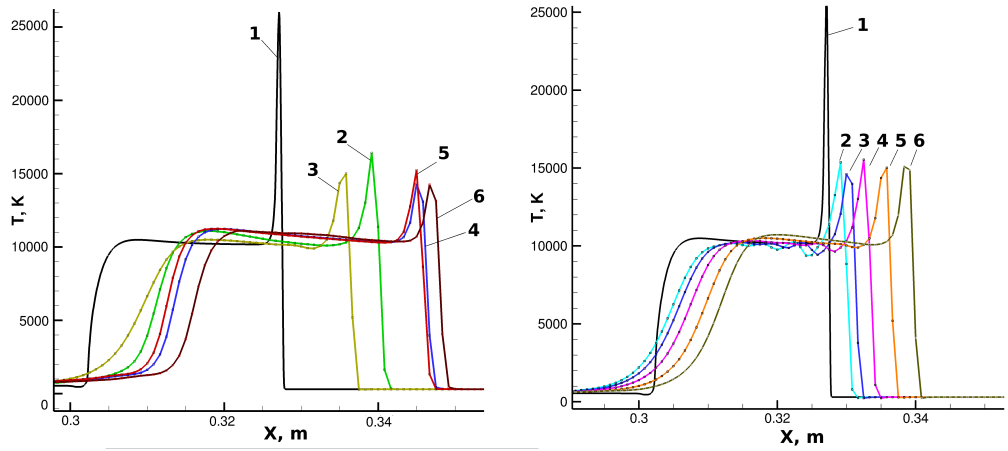

FIGURE 9. 1D, 13 species EAST problem: Comparison among methods using 601 point grids with $CFL = 0.6$ and $t_{end} = 3.25\times10^{-5}$ *sec*. Left subfigure: Reference solution (TVD on a 10,001 point grid) (line 1), TVD (line 2), ACMTVDfi (TVDfi) using $\kappa = 0.5$ (line 3), WENO5-llf (line 4), WENO5P-llf (line 5), WENOPH-llf (line 6). Right: ACMTVDfi, $\kappa = 0.15$ (line 2), $\kappa = 0.2$ (line 3), $\kappa = 0.3$ (line 4), $\kappa = 0.5$ (line 5), $\kappa = 1$ (line 6). See text for method notation.

Department of Energy by Lawrence Livermore National Laboratory under Contract DE-AC52-07NA27344.

REFERENCES

GRIFFITHS, D., STUART, A. & YEE, H. 1992 Numerical wave propagation in hyperbolic problems with nonlinear source terms. *SIAM J. Numer. Anal.* **29**, 1244–1260.

HU, X. Y., ADAMS, N. A. & SHU, C.-W. 2012 Positivity-preserving flux limiters for high-order conservative schemes. arXiv:1203.1540v4, preprint submitted to Elssvier.

JIANG, G. S. & SHU, C. W. 1996 Efficient implementation of weighted ENO schemes. *J. Comp. Phys.* **126**, 202–228.

LAFON, A. & YEE, H. 1996 Dynamical approach study of spurious steady-state numerical solutions for nonlinear differential equations, part III: The effects of nonlinear source terms in reaction-convection equations. *Comput. Fluid Dyn.* **6**, 1–36.

LEVEQUE, R. & YEE, H. C. 1990 A study of numerical methods for hyperbolic conservation laws with stiff source terms. *J. Comp. Phys.* **86**, 187–210.

NOH, W. F. 1987 Errors for calculations of strong shocks using artificial viscosity and an artificial heat flux. *J. Comput. Phys.* **72**, 78–120.

SEDOV, L. I. 1959 *Similarity and Dimensional Methods in Mechanics*. New York: Academic Press.

SHU, C. W. & OSHER, S. 1988 Efficient implementation of essentially nonoscillatory shock-capturing schemes. *J. Comp. Phys.* **77**, 439471.

WANG, W., SHU, C., YEE, H. C. & SJÖGREEN, B. 2012 High order finite difference methods with subcell resolution for advection equations with stiff source terms. *J. Comput. Phys.* **231**, 190–214.

YEE, H. C. 1989 *A class of high-resolution explicit and implicit shock-capturing methods*. VKI lecture series 1989-04.

YEE, H. C., KLOPFER, G. H. & MONTAGNE, J.-L. 1990 High-resolution shock-

capturing schemes for inviscid and viscous hypersonic flows. *J. Comput. Phys.* **88**, 31–61.

Yee, H. C., Kotov, D. V., Wang, W. & Shu, C.-W. 2012 Spurious behavior of shock-capturing methods: Problems containing stiff source terms and discontinuities. In *Proceedings of the ICCFD7*. The Big Island, Hawaii.

Yee, H. C., Sandham, N. & Djomehri, M. 1999 Low dissipative high order shock-capturing methods using characteristic-based filters. *J. Comput. Phys.* **150**, 199–238.

Yee, H. C. & Sjögreen, B. 2007 Development of low dissipative high order filter schemes for multiscale Navier-Stokes/MHD systems. *J. Comput. Phys.* **225**, 910–934.

Yee, H. C. & Sjögreen, B. 2010 High order filter methods for wide range of compressible flow speeds. In *Proc. of ASTRONUM-2010*. San Diego, Calif, expanded version submitted to Computers & Fluids.

Zhang, X. & Shu, C.-W. 2010 On positivity preserving high order discontinuous galerkin schemes for compressible Euler equations on rectangular meshes. *J. Comput. Phys.* **229**, 8918–8934.

Zhang, X. & Shu, C.-W. 2012 Positivity-preserving high order finite difference WENO schemes for compressible Euler equations. *J. Comput. Phys.* **231**, 2245–2258.